

Charged basal stacking fault (BSF) scattering in nitride semiconductors

Aniruddha Konar,^{1,2, a)} Tian Fang,^{3,2} Nan Sun,¹ and Debdeep Jena^{3,2}

¹⁾Department of Physics, University of Notre Dame, Notre Dame, USA 46556

²⁾Midwest Institute of Nanoelectronics Discovery (MIND), Notre Dame, USA 46556

³⁾Department of Electrical Engineering, University of Notre Dame, Notre Dame, USA 46556

(Dated: 5 September 2022)

A theory of charge transport in semiconductors in the presence of basal stacking faults is developed. The work is directed to the understanding of carrier transport in non-polar GaN film consisting of a large number of extended defects. The anisotropy in carrier transport predicted by theory is in reasonable agreement with experiments.

The III-V nitride semiconductors and related compounds have attracted an immense attention for optoelectronic devices^{1,2} covering a wide range of the electromagnetic spectrum as well as high-speed, high temperature electronics devices. For c-plane grown nitrides, built-in polarization field, although advantageous for two dimensional electron gas (2DEG) formation in transistors³, reduces overlap of electron-hole wavefunction in addition to the redshift in optical transition. Moreover, c-plane based enhancement mode (E-mode) transistors suffer from low threshold voltage ($V_{th} \sim 1$ V) impeding its application in safe circuit operation. A potential way to eliminate these effects is to grow nitrides in non-polar direction. A good quality non-polar film, however still remains elusive. Heteroepitaxial, non polar and semi-polar nitrides films grown on lattice mismatched substrates, contain 1-10 $\times 10^5$ /cm basal stacking faults (BSFs) parallel to the [0001] direction⁴⁻⁶. Directionally dependent transport measurements in highly faulted non-polar nitride films show strong anisotropy for electrons and holes, with [0001] parallel mobility reduced relative to the in-plane [1120]⁷⁻⁹. This anisotropy has been associated with scattering from BSFs qualitatively, although no theoretical effort of modeling scattering from BSFs has been made so far. In this letter, we developed a theory of carrier scattering phenomena from BSFs and a quantitative estimate of transport anisotropy is predicted.

The stacking fault (SF) primarily results from the large density of structural defects associated with heteroepitaxial growth on lattice-mismatched substrates. Most prevalent SF in wurtzite (WZ) nitrides is of I_1 -type requiring lowest energy of formation¹⁰. The scattering contrast transmission microscope (TEM) imaging revealed⁴ that the SF are primarily I_1 -type which corresponds to a stacking sequence of (0001) basal plane $\dots ABABABCBCBC \dots$. ABC stacking in the fault region indicates that, indeed a BSF can be thought as a perfect insertion of thin zincblende (ZB) structure (up to three monolayers) in the WZ matrix as shown in Fig.1a). The built-in polarization difference between ZB and WZ

structures will result in bound sheet charges $\pm\sigma_\pi$ at each interfaces of BSFs. Consequently, the band edge will bend around the fault region. Fig.1b) shows a typical conduction band diagram around a BSF for a n-doped GaN film along with the charges that are formed each interfaces of the homojunction. The bending of conduction band edge inside the fault region is due the electric field resulting from polarization bound charge, whereas, band bends outside the BSF due to the accumulation and depletion of mobile charges. We approximate the accumulation charge as a sheet charge of density n_s at the centroid (t) of the charge distribution, i.e. $\rho_\pi(x) = en_s\delta(x - x_0)$, where $x_0 = d + t$, d being the width of the fault region. If x_d is the width of the depletion region, charge neutrality gives $n_s = x_d N_d$, where N_d is the donor density. The energy conservation across the fault region leads to the relation

$$\frac{eN_d x_d^2}{2\epsilon_s} + \frac{en_s t}{2\epsilon_s} = \left(\frac{e\sigma_\pi}{2\epsilon_s} - \frac{en_s}{2\epsilon_s} \right) d \quad (1)$$

, where, ϵ_s is the permittivity of the semiconductor. In the limit, $x_d \gg (t, d)$, the depletion length is $x_d \simeq \sqrt{\sigma_\pi d / N_d}$. Depletion width x_d increases with decreasing donor density and there exists a critical donor density

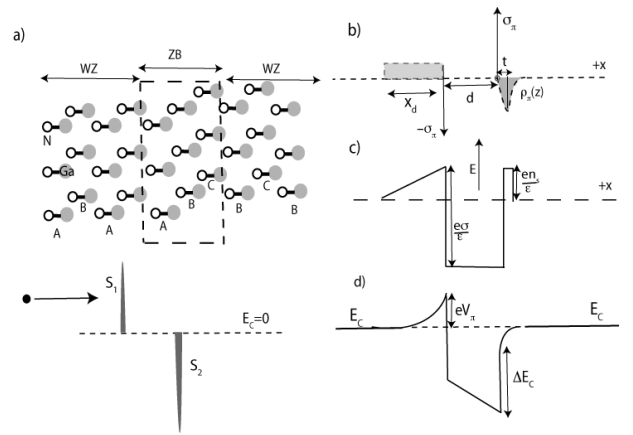


FIG. 1. a) structure of basal stacking faults , b) schematic charge across the basal stacking fault, c) schematic diagram of electric field, d) conduction band diagram including band-offset, e) delta-function model of barrier and QW.

a) akonar@nd.edu

71 N_d^{cr} for which, x_d is comparable to the distance between
 72 two stacking faults. As a results the whole channel is
 73 depleted, and the conduction ceases along x direction.
 74 If n_{SF} is the fault density, the critical donor density
 75 at which onset of conduction along x direction occurs
 76 is given by $N_d^{cr} = \sigma dn_{SF}^2$. For a typical fault density
 77 $n_{SF} = 10^5/\text{cm}$ and $d = 0.8$ nm for GaN, critical doping
 78 density is $N_d^{cr} = 10^{16}/\text{cm}^3$. In the rest of the paper, we
 79 will work in the regime where $N_d \gg N_d^{cr}$.
 80 In addition to the polarization charges at interfaces, con-
 81 duction band offset (ΔE_c) between ZB and WZ struc-
 82 tures leads to a deep quantum well (QW) in the fault re-
 83 gion as shown in Fig.1b). For an applied bias, electrons
 84 tunnel through the barrier (in the depletion region) and
 85 QW (in the fault region) and then diffuse in the space
 86 between two consecutive stacking faults. To model the
 87 transmission coefficient of tunneling, we approximate the
 88 barrier and the QW as two delta functions (as shown in
 89 Fig.1e) of strengths $S_1 = eV_\pi x_d$ and $S_2 = (\Delta E_c + eV_\pi)d$;
 90 where $V_\pi = \sigma_\pi d/2\epsilon_s$. The energy dependent coefficient of
 91 transmission through a single delta function potential is
 92 a analytically solvable problem and can be found in stan-
 93 dard textbook of quantum mechanics¹¹. If $T_{tr,1}(\epsilon)$ and
 94 $T_{tr,2}(\epsilon)$ are the transmission coefficient from the barrier
 95 and QW, then total coefficient of transmission across the
 96 fault region is given by $T_{tr}(\epsilon) = T_{tr,1}(\epsilon)T_{tr,2}(\epsilon)$; where

$$T_{tr}(\epsilon) = \left[\frac{1}{1 + \frac{m^* S_1^2}{2\hbar^2 \epsilon}} \right] \times \left[\frac{1}{1 + \frac{m^* S_2^2}{2\hbar^2 \epsilon}} \right], \quad (2)$$

97 where, ϵ is the energy of the incoming electron and m^*
 98 is the effective mass at the band edge. In SF-free struc-
 99 tures, the elemental current component along x direction
 100 for an electron with velocity v_k is given by $j_k^x = e\delta f_k v_k^x$;
 101 where δf_k is the modification of equilibrium Fermi-Dirac
 102 distribution caused by an applied electric field F_{appl} . In
 103 the presence of SFs, a part (given by Eq. 2) of these car-
 104 riers is transmitted through the barrier and QW leading
 105 to an effective elemental current density $j_k^{eff} = T_{tr}(\epsilon)j_k^x$.
 106 Then, total current density in the presence of SF is given
 107 by

$$J_x = 2e \int \frac{d^3k}{(2\pi)^3} T_{tr}(\epsilon) \delta f_k v_k^x, \quad (3)$$

108 where, v_k^x is the x component of electron's group ve-
 109 locity in the state $|\mathbf{r}, \mathbf{k}\rangle$ and the factor 2 takes account
 110 the spin degeneracy. For a small applied electric field
 111 along x direction, under relaxation time approximation
 112 (RTA), $\delta f_k = (-\partial f_0/\partial \epsilon)\tau(k)v_k^x F_{appl}$, where, f_0 is the
 113 equilibrium Fermi-Dirac distribution function and $\tau(k)$
 114 is the momentum relaxation time corresponding to con-
 115 ventional disorders (impurity, phonons etc) present in the
 116 material. Integrating Eq.3 over all k -space and defining
 117 conductivity by the relation $J_x = \sigma(n, T)F_{appl}$, one ob-
 118 tains carrier concentration (n) and temperature (T) de-
 119 pendent conductivity in presence of BSFs. The expres-

sion for conductivity across the BSF is given by

$$\sigma_{xx}(T, n) = \frac{3ne^2 \int d\epsilon \epsilon^{1/2} \cosh^{-2}(\epsilon/2k_B T) T_{tr}(\epsilon) \tau(\epsilon) v_x^k v_x^k}{8\pi \int d\epsilon \epsilon^{3/2} \cosh^{-2}(\epsilon/2k_B T) d\epsilon}, \quad (4)$$

121 where T is the equilibrium temperature, k_B is Boltzmann
 122 constant. By inserting $T_{tr}(\epsilon) = 1$ for all energies, a sim-
 123 ilar expression can be obtained for conductivity (σ_{yy})
 124 along the y direction. Moreover, an analogous band dia-
 125 gram and transport formalism can be developed for hole
 126 transport. For hole transport, ΔE_c should be replaced
 127 by valence band offset (ΔE_v) in the strength of delta
 128 function potentials S_1 and S_2 , and an hole effective mass
 129 should be used instead of electron effective mass.
 130 Equation (4) is the central finding of this work as it allows
 131 to calculate experimentally measurable quantities such
 132 as conductivity and mobility in the presence of BSFs.
 133 As an application of the formalism constructed above as
 134 well as availability of experimental data in existing liter-
 135 ature, we investigate charge transport in faulted m -plane
 136 (1 $\bar{1}$ 00) GaN. We first investigate the hole transport in
 137 p-doped m -plane GaN film. Inclusions of different scat-
 138 tering mechanisms are necessary to evaluate energy de-
 139 pendent momentum relaxation time $\tau(\epsilon)$ appearing in
 140 Eq. 4. Due to high activation energy of acceptors (Mg
 141 for p-type GaN has activation energy ~ 174 meV), most
 142 of the dopant remains neutral even at room tempera-
 143 ture acting as scatterers to hole. The fact that a high
 144 doping density is required to achieve appreciable hole
 145 concentrations, results in high density of neutral impu-
 146 rities (NI) making neutral impurity scattering dominant
 147 even at room temperature. Accounting zero-order phase
 148 shift¹², the momentum relaxation time of neutral impu-
 149 rity scattering is $\tau_{NI}^{-1} = 20N\hbar a_0/m^*$; where N is the den-
 150 sity of neutral impurities and $a_0 = 4\pi\epsilon_s\hbar^2/m^*e^2$ is the
 151 effective Bohr radius. Momentum relaxation time (τ_{im})
 152 due to ionized impurity scattering is calculated following
 153 the method of Brooks-Herring (BH) technique¹³. The
 154 fact that $\tau_{imp} \sim n_{imp}^{-1}$; where n_{imp} is the density of ion-
 155 ized impurities, makes ionized impurity scattering impor-
 156 tant at high carrier concentrations (ionized dopant con-
 157 centrations). For electron-optical phonon momentum-
 158 relaxation time (τ_{ph}), only phonon absorption has been
 159 considered due to high optical phonon energy ($E_{op} =$
 160 0.092 eV $\gg k_B T$) of GaN. The resultant momentum-
 161 relaxation time is calculated using Mathiessen's rule; i.e.
 162 $\tau(\epsilon)^{-1} = \tau_{NI}^{-1} + \tau_{imp}^{-1} + \tau_{ph}^{-1}$. For numerical calculations,
 163 we assume valence band offset $\Delta E_v = 0.06$ meV¹⁰. The
 164 hole effective mass of GaN is not well known and a wide
 165 range of $m_h^* = 0.4 - 2.4m_0$ ² (m_0 is the rest mass of a
 166 bare electron) is found in existing literatures. For best
 167 illustration, in our work, we assume hole effective mass
 168 $m_h^* = 1.8m_0$. Neutral impurity density is chosen to
 169 be $N = 24 \times p$, where p is free hole concentration in
 170 GaN. This choice of neutral impurity density is not ad
 171 hoc; measurement⁷ shows that neutral impurity density
 172 $N = N_A - p \approx 20 - 25 \times p$ for a wide range of acceptor
 173 density N_A . Figure 2a) shows the variation of σ_{xx} (along

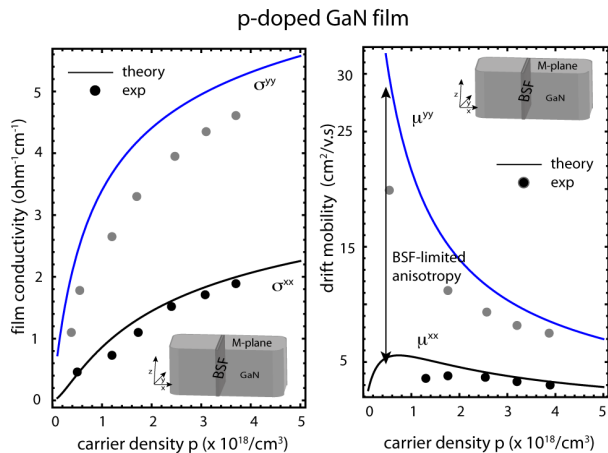


FIG. 2. a) hole conductivity as a function of hole density: anisotropy is due to BSF b) hole mobility as a function of hole density. solid lines are theoretical values and solid circles are experimental values extracted from ref. 7.

the c -axis) and σ_{yy} (parallel to a axis) as a function of hole density at room temperature. It is apparent from the figure that the presence of BSF causes an appreciable reduction of σ_{xx} compare to σ_{yy} , resulting anisotropic hole transport. Defining hole mobility as $\mu_{ii} = \sigma_{ii}/pe$; $i = x, y$, corresponding hole mobility is also anisotropic as shown in Fig.2b). The anisotropy in hole mobility increases with decreasing hole density. This stems out from the fact that, in the limit $p \rightarrow 0$, depletion width increases ($x_d \sim N_A^{-1/2}$) and one approaches to the critical acceptor density limit N_A^{cr} . As x_d increases, strength of the barrier S_1 increases, such that $T_{tr}(\epsilon) \approx 0$; results in vanishing μ_{xx} (σ_{xx} ; see Fig.2) whereas, contribution from free holes in accumulation region leads to a finite (low but non-vanishing) conductivity (mobility) along y direction.

To corroborate the above idea of BSF induced transport anisotropy in GaN, we further investigate the electron transport in n-doped samples in the presence of BSF. Experiment⁷ shows that electron mobility in m-GaN sample decreases with decreasing electron concentration. This phenomena is well described by charged dislocation scattering as pointed out by Weimann et. al¹⁴. Large lattice mismatch between GaN and substrate (for GaN on SiC lattice mismatch $\sim 2.9\%$) leads to high dislocation densities. For a m-plane GaN grown on foreign substrate, TEM image reveals^{15,16} edge dislocation lines perpendicular to m-plane (along $[1\bar{1}00]$ direction) with non zero Burger's vector along $[0001]$ direction. Each dislocation line acts as an acceptor like trap with a line charge density $\rho_L = e/a$, where a is the a -lattice constant of GaN. The electrons moving in the perpendicular plane to the dislocation line effectively feel a Coulomb potential $V(r) = (\rho_L/2\pi\epsilon_s)K_0(r/L_D)$, where $K_0(\dots)$ is the zeroth order Bessel function of 2nd kind and $L_D = \sqrt{k_B T \epsilon_s / e^2 n'}$ is the Debye screening length. Both free electrons, and bound electrons are taken account in

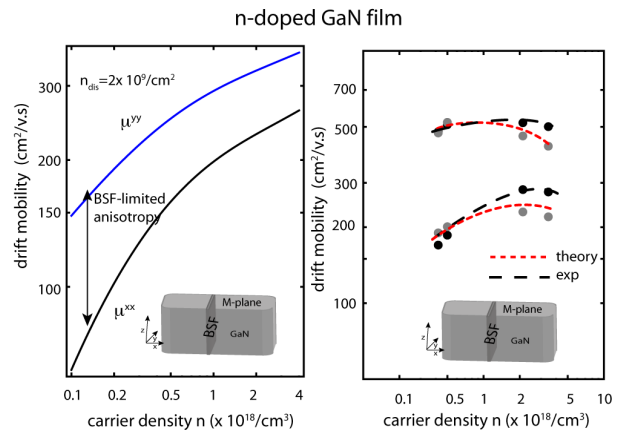


FIG. 3. a) electron mobility as a function of electron density, b) comparison between theoretical values (dotted line) and experimental values (dashed line) of electron mobility at different values of electron concentrations.

the effective screening concentration (n') using Brook's¹⁷ formula $n' = 2n - n^2/N_D$; where n is the free carrier concentration. The momentum relaxation time (τ_{dis}) due to dislocation lines has been calculated by several authors for three^{14,18,19} and two-dimensional electron gas²⁰ in GaN. In the presence of BSF, the x component of conductivity at room temperature due to dislocation scattering can be calculated as

$$\sigma_{xx}^{dis} = \left(\frac{\epsilon_s}{e^2}\right)^2 \frac{3ne^2 a^2 (k_B T)^{3/2}}{4\pi\sqrt{m^*} n_{dis} L_D} \mathcal{I}(n, \Delta E_c), \quad (5)$$

where, n_{dis} is the dislocation density and $\mathcal{I}(n, \Delta E_c)$ is a dimensionless integral. The complex nature of the integral $\mathcal{I}(n, \Delta E_c)$ render us to evaluate analytically and one must rely on numerical techniques. For $\Delta E_c = 0.27$ eV¹⁰, and in the non-degenerate limit $\mathcal{I}(n, 0.27) \simeq 6$, and $\mu_{xx} \sim \sqrt{n}$. Fig. 3a) shows room temperature drift mobility with electron density for dislocation density $n_{dis} = 2 \times 10^9/\text{cm}^2$. It not only captures mobility anisotropy due to BSF, but also the mobility variation with carrier concentration is similar to those measured experimentally^{7,14}. For calculations, we used $m_{xx}^* = m_{yy}^* = 0.22m_0$, and a resultant momentum relaxation time $\tau^{-1} = \tau_{dis}^{-1} + \tau_{NI}^{-1} + \tau_{imp}^{-1} + \tau_{ph}^{-1}$ is assumed. Unlike p-doped GaN, the neutral impurity in n-doped samples comes from unintentionally doped C atom with measured density $N \sim 5 \times 10^{16}/\text{cm}^2$. Though the assumption of a fixed dislocation density explains experimentally observed mobility variation and anisotropy reasonably well, it is unlikely though, that different samples would contain same dislocation density. Moreover, a careful estimation of dislocation density is necessary to compare the theory with experimental data. Experiment⁷ shows free electron concentration using Hall technique is significantly lower than actual dopant concentration in n-doped GaN samples. The origin of this difference coming from unactivated dopants is unlikely; we rather attribute it to the

TABLE I. Dislocation density for various n-dope GaN. Parameters have been taken from ref.⁷.

| | $N_D (\times 10^{18})$ (cm^{-3}) | $n (\times 10^{18})$ (cm^{-3}) | $n_{dis} (\times 10^8)$ (cm^{-2}) |
|----|--|--|---|
| 1. | 1.40 | 0.41 | 2.8 |
| 2. | 1.87 | 0.5 | 2.8 |
| 3. | 5.60 | 2.5 | 2.0 |
| 4. | 10.0 | 3.06 | 9.1 |

acceptor traps associated with dislocation lines. Moreover, the difference $(N_D - n) \sim n_{dis}$ varies from sample to sample indicating sample dependent density of dislocations. Assuming a single trap per a-axis, volume density of trapped charge is n_{dis}/a ; and a charge balance equation can be written as

$$n + \frac{n_{dis}}{a} = \frac{N_D}{1 + \frac{n}{2N_C} \exp(E_D/k_B T)}, \quad (6)$$

where, $N_C = 2(m^*k_B T/2\pi\hbar^2)^{3/2}$ is the effective density of states and E_D is the activation energy of the donor level. The screening effect on the donor activation energy is taken account by the empirical formula $E_D = E_{D0} - \alpha N_D^{1/3}$ ²¹, where screening parameter $\alpha = 2.1 \times 10^{-5}$ meV.cm and $E_{D0} = 28$ meV²¹. Using Eq. 6 and values of N_D and n from ref. 7 calculated dislocation densities are tabulated in Table I. Electron mobilities using the values of dislocation densities of Table I is determined and compared to experimentally measured values as shown in Fig. 3b). At low carrier densities, theoretical values are at well accordance with experimental one; but differ significantly at high carrier concentrations. We speculate this disagreement is due to the use of classical Debye screening function. At high carrier densities, electron gas behaves degenerately and use of full quantum screening function would result in better agreement between theory and experiments. Moreover, one should not consider this agreement (disagreement) between theory and experimental data too strictly for two reasons ... i) there is not enough data points for comparison and ii) extraction of data points can be quite erroneous²². While the procedure described above serves as a guideline for comparing theory with the measurements, availability of more measured data in future would result in a better justification of the theory.

An important observation is that the anisotropy in electron and hole mobilities decreases with increasing carrier concentration. At higher carrier densities, transmission of carriers occupying higher energy states approaching to the maximum limit ($T_{tr}(\epsilon) \rightarrow 1$) leading to the fact $\mu_{xx} \rightarrow \mu_{yy}$. The corresponding carrier density is $n_0(p_0) \simeq 1/3\pi^2(m^*\Delta E_c/\hbar^2)^3$, beyond which BSF-induced transport anisotropy vanishes in non-polar GaN. At high acceptor concentration, energy levels of impurity atoms overlaps to form impurity band. While conduction through this impurity band is important at low temperatures; at room temperature impurity band does not form

an efficient transport path²³ and its exclusion from our model is quite justified. Also, the comparison between theoretically calculated drift mobility and experimentally measured Hall mobility is meaningful as at room temperature, the Hall factor $r_H \sim 1$ ²¹. Our work presented here can be improved in three ways ... i) At low carrier densities x_d is large; assumption of delta function barrier breaks down and one should solve Schrodinger equation numerically to obtain exact transmission coefficient $T_{tr1}(\epsilon)$, and ii) at low doping level (when x_d is large) or for high stacking fault density, carriers are confined in a quasi-two dimensional space rather than moving in three dimensions. Hence, one should use a two-dimensional analogue of Eq.4 for an exact evaluation of μ_{yy} , and iii) by incorporating the contributions of quasi-localized electrons in the shallow state of the thin QW located in the fault region.

The theory presented here is not only applicable to GaN, but to any semiconductor having BSFs with proper insertion of material parameters. For example, ZnO shows SF similar to GaN with $\sigma_\pi = .057$ C/m² and band offsets²⁴ are $\Delta E_c = 0.147$ eV and $\Delta E_v = 0.037$ eV.

In summary, we have presented a transport theory in semiconductors containing a large degree of basal stacking faults. The theory is applied to understand the experimentally observed transport anisotropy in faulted m-plane GaN and a reasonable agreement between theory and experiment is obtained. Two critical limits of carrier concentration is derived, one where transport across a basal stacking fault ceases and another, where presence of basal stacking faults can be ignored in the context of charge transport.

The authors would like to acknowledge J. Verma, S. Ganguly (University of Notre Dame) for helpful discussions and National Science Foundation (NSF), Midwest Institute for Nanoelectronics Discovery (MIND) for the financial support for this work.

¹P. Waltereit *et al.* Nature **406**, 865 (2000).

²J. Piprek, *Nitride Semiconductor Devices: Principles and Simulations* (Wiley-VCH, Weinheim, 2007).

³C. Wood and D. Jena, *Polarization Effects in Semiconductors: From Ab Initio Theory to Device Applications* (Springer, NY, 2008).

⁴B. A. Haskell *et al.*, J. Electron. Mater. **34**, 357 (2005).

⁵C. Hsiao *et al.*, J. Appl. Phys. **107**, 073502 (2010).

⁶K. Ueno, A. Kobayashi, J. Ohta and H. Fujioka, Jpn. J. Appl. Phys. **49**, 060213 (2010).

⁷M. McLaurin, T. E. Mates, F. Wu and J. S. Speck, J. Appl. Phys. **100**, 063707 (2006).

⁸M. McLaurin, T. E. Mates, and J. S. Speck, Phys. Stat. Sol. (RRL), **1**, 110 (2007).

⁹K. H. Baik *et al.*, IEEE. Photon. Technol. Lett. **22**, 595 (2010).

¹⁰C. Stampfl and C. G. Van de Walle, Phys. Rev. B. **24**, R15052 (1998).

¹¹D. J. Griffiths, *Introduction to Quantum Mechanics* (Pearson Education Inc. Singapore, 2005).

¹²C. Erginsoy, Phys. Rev. **79**, 1013 (1950).

¹³H. Brooks, Phys. Rev. **83**, 879 (191).

¹⁴N. G. Weimann and L. F. Eastman, J. Appl. Phys. **83**, 3656 (1998).

¹⁵I. Lo *et al.*, Appl. Phys. Lett. **92**, 2020106 (2008).

- ¹⁶D. N. Zakharov and Z. Liliental-Webber, Phys. Rev. B. **71**, 235334 (2005).
- ¹⁷K. Seeger, *Semiconductor Physics: An Introduction*, 7th Ed. pp-173, (Springer, New York, 1999).
- ¹⁸B. Pödör, Phys. Stat. Sol. **16**, K167 (1966).
- ¹⁹D. C. Look and J. R. Sizelove, Phys. Rev. Lett. **82**, 1237 (1998).
- ²⁰D. Jena, A. C. Gossard and U. K. Mishra, Appl. Phys. Lett. **76**, 1707 (2000).
- ²¹D. C. Look *et al.*, Solid State. Comm. **102**, 297 (1997).
- ²²Data is extracted from a log-log plot reported in ref. 7 using the MATLAB code available at <http://cobweb.ecn.purdue.edu/~lundstro/publications/ReadData.m>. Due to finite size of the experimental data points, extraction from log-log plot can introduce significant error. For hole brach, this is error is small due to linear scale of the plot.
- ²³D. Lancefield and H. Eshghi, J. Phys.: Condens. Matter **13**, 8939 (2001).
- ²⁴Y. Yan *et al.*, Phys. Rev. B. **70**, 193206 (2004).